Memristive Devices and Systems

LEON O. CHUA, FELLOW, IEEE, AND SUNG MO KANG, MEMBER, IEEE

Abstract—A broad generalization of *memristors*—a recently postulated circuit element—to an interesting class of nonlinear dynamical systems called *memristive systems* is introduced. These systems are unconventional in the sense that while they behave like resistive devices, they can be endowed with a rather exotic variety of dynamic characteristics. While possessing memory and exhibiting small-signal inductive or capacitive effects, they are incapable of energy discharge and they introduce no phase shift between the input and output waveforms. This zero-crossing property gives rise to a Lissajous figure which always passes through the origin. Memristive systems are hysteretic in the sense that their Lissajous figures vary with the excitation frequency. At very low frequencies, memristive systems are indistinguishable from *nonlinear* resistors while at extremely high frequencies, they reduce to *linear* resistors. These anomalous properties have misled and prevented the identification of many memristive devices and systems—including the thermistor, the Hodgkin-Huxley membrane circuit model, and the discharge tubes.

Generic properties of memristive systems are derived and a *canonic dynamical system model* is presented along with an explicit algorithm for identifying the model parameters and functions.

I. Introduction

THE MEMRISTOR has been postulated recently as the fourth basic circuit element [1]. This element behaves like a linear resistor with memory but exhibits many interesting nonlinear characteristics. These unconventional properties have led to the successful modeling of a number of physical devices and systems [1]–[4]. Notwithstanding these applications, however, there remains an even broader class of physical devices and systems whose characteristics resemble those of the memristor and yet cannot be realistically modeled by this element, the reason being that the memristor is only a special case of a much more general class of dynamical systems—henceforth called *memristive systems*—defined by[1]

$$\boxed{\begin{aligned} \dot{x} &= f(x, u, t) \\ y &= g(x, u, t)u \end{aligned}} \tag{1}$$

where u and y denote the *input* and *output* of the system and x denotes the *state* of the system. The function $f: \mathcal{R}^n \times \mathcal{R} \times \mathcal{R} \rightarrow \mathcal{R}^n$ is a continuous n-dimensional vector function and g: $\mathcal{R}^n \times \mathcal{R} \times \mathcal{R} \rightarrow \mathcal{R}$ is a continuous scalar function. It is assumed that the state equation in (1) has a unique solution for any initial state $x_0 \in \mathcal{R}^n$. The output equation in (1) is such that the output y is equal to the product between the input u and the scalar function g. This special structure of the readout map is what distinguishes a memristive system from an arbitrary *dynamical system* [5]; namely, the output y is zero whenever the input u is zero, regardless of the state x which incorporates the memory effect. This *zero-crossing* property manifests itself vividly in the form of a Lissajous figure which always passes through the origin.

An nth-order[2] current-controlled memristive one-port is represented by

$$\begin{aligned} \dot{x} &= f(x, i, t) \\ v &= R(x, i, t)i \end{aligned} \tag{2}$$

and an nth-order voltage-controlled memristive one-port is represented by

$$\begin{aligned} \dot{x} &= f(x, v, t) \\ i &= G(x, v, t)v \end{aligned} \tag{3}$$

where v and i denote the port voltage and current, respectively. The functions f, R, or G are similarly defined as f, g in (1). In the special case when the one-port is time-invariant[3] and R(resp. G) is not an explicit function of i(resp. v) we have

$$\begin{aligned} \dot{x} &= f(x, i) \quad (\text{resp.}, \dot{x} = f(x, v)) \\ v &= R(x)i \quad (\text{resp.}, i = G(x)v). \end{aligned} \tag{4}$$

To motivate the significance of memristive systems, we pause to present some examples of physical devices which should be modeled as memristive one-ports, but which have so far been improperly identified.

Example 1—Thermistor

Thermistors have been widely used as a linear resistor whose resistance varies with the ambient temperature [6]. In particular, a *negative-temperature coefficient* thermistor is characterized by [7]

$$v = R_0(T_0) \exp\left[\beta\left(\frac{1}{T} - \frac{1}{T_0}\right)\right] i \triangleq R(T)i \tag{5}$$

where β is the material constant,[4] T is the absolute body temperature of the thermistor, and T_0 is the ambient temperature in kelvin. The constant $R_0(T_0)$ denotes the cold temperature resistance at $T = T_0$. The instantaneous temperature T, however, is known to be a function of the power dissipated in the thermistor and is governed by the heat transfer equation

$$p(t) = v(t)\, i(t) = \delta(T - T_0) + C\frac{dT}{dt} \tag{6}$$

where C is the heat capacitance and δ is the dissipation constant[5] of the thermistor which is defined as the ratio of a

Manuscript received May 15, 1975; revised August 4, 1975. This work was supported by the Naval Electronic Systems Command under Contract N00039-75-C-0034, the Joint Services Electronics Program under Contract F44620-71-C-0087, and the National Science Foundation under Grant GK-32236x1.

L. O. Chua is with the Department of Electrical Engineering and Computer Sciences and the Electronics Research Laboratory, University of California, Berkeley, CA 94720.

S. M. Kang is with the Department of Electrical Engineering, Rutgers University, New Brunswick, NJ 08901.

[1] The extension of this definition to the *multiport* case is straightforward. Hence, only the one-port case will be discussed in this paper.

[2] The number n denotes the dimension of the state space of the dynamical system.

[3] The dynamical system (1) is said to be *time-invariant* if both f and g are not explicit functions of time t.

[4] Although β increases slightly with increasing temperature, it may be approximated by a constant over the temperature range of interest.

[5] Strictly speaking, δ is not a true constant, but varies slightly with both T_0 and $T - T_0$. However, for simplicity, δ is assumed to be constant here.

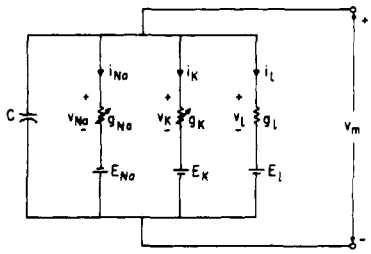

Fig. 1. The Hodgkin-Huxley model.

change in the power dissipation to the resultant change in the body temperature. Substituting (5) into (6) and by rearranging terms, we obtain

$$\frac{dT}{dt} = -\frac{\delta}{C}(T - T_0) + \frac{R_0(T_0)}{C}\exp\left[\beta\left(\frac{1}{T} - \frac{1}{T_0}\right)\right] i^2 \triangleq f(T, i). \tag{7}$$

We observe from (5) and (7) that *a thermistor is* in fact not a memoryless temperature-dependent linear resistor—as is usually assumed to be the case—but rather *a first-order time-invariant current-controlled memristive one-port*.

Example 2—Ionic Systems

The celebrated Hodgkin–Huxley circuit model [8] of the nerve axon membrane is shown in Fig. 1. Hodgkin and Huxley described the potassium channel conductance g_K and the sodium channel conductance g_{Na} as *time-varying conductances* whose variations are functions of the solutions of first-order differential equations. The potassium channel is described by

$$i_K = \bar{g}_K n^4 v_K \triangleq G_K(n) v_K$$

$$\dot{n} = \frac{0.01(v_K + E_K + 10)}{\exp[(v_K + E_K + 10)/10] - 1}(1 - n) - 0.125\exp\left(\frac{v_K + E_K}{80}\right) n \triangleq f(n, v_K) \tag{8}$$

where $\bar{g}_K$ and E_K are constants. The sodium channel is described by

$$i_{Na} = \bar{g}_{Na} m^3 h v_{Na} \triangleq G_{Na}(m, h) v_{Na}$$

$$\dot{m} = \frac{0.1(v_{Na} - E_{Na} + 25)}{\exp[(v_{Na} - E_{Na} + 25)/10] - 1}(1 - m) - 4\exp\left(\frac{v_{Na} - E_{Na}}{18}\right) m \triangleq f_1(m, v_{Na}) \tag{9}$$

$$\dot{h} = 0.07\exp\left(\frac{v_{Na} - E_{Na}}{20}\right)(1 - h) - \frac{1}{\exp[(v_{Na} - E_{Na} + 30)/10] + 1} h \triangleq f_2(h, v_{Na})$$

where $\bar{g}_{Na}$ and E_{Na} are constants. It follows from (8) and (9) that since the time-varying conductances cannot be specified as an *a priori* function of time, they are actually memristive systems. In particular, *the potassium channel of the Hodgkin-Huxley model should be identified as a first-order time-invariant voltage-controlled memristive one-port and the sodium channel should be identified as a second-order time-invariant voltage-controlled memristive one-port.*

Example 3—Discharge Tubes

Francis [9] described the behaviors of discharge tubes by

$$\dot{n} = \alpha i v - \beta n \tag{10a}$$

$$v = \frac{F}{n} i \triangleq R(n) i \tag{10b}$$

where α, β, and F are constants depending on the dimensions of the tubes and the gas fillings. The variable n denotes the electron density of the tubes. Substituting (10b) into (10a) we obtain

$$\dot{n} = \frac{\alpha F}{n} i^2 - \beta_n \triangleq f(n, i). \tag{10c}$$

It follows from (10b) and (10c) that *the discharge tube should also be modeled as a first-order time-invariant current-controlled memristive one-port*. It is unfortunate that while researchers have long regarded such discharge tubes as neon bulbs and fluorescent lamps as dynamic devices, they have failed to recognize their memristive properties.

II. Generic Properties of Memristive One-Ports

Since many memristive devices have been incorrectly classified, our next objective will be to derive the *generic* properties which clearly distinguish a memristive device from other systems. For simplicity, we will restrict our study to current-controlled memristive one-ports.[6]

Property 1—Passivity Criterion[7]

Let a current-controlled memristive one-port be time-invariant and let its nonlinear function $R(\cdot)$ associated with the readout map satisfy the constraint $R(x, i) = 0$ only if $i = 0$. Then the one-port is *passive* if and only if $R(x, i) \geqslant 0$ for any admissible input current $i(t)$, for all $t \geqslant t_0$, where t_0 is chosen such that $x(t_0) = x^*$, where x^* is the state of *minimum energy storage* [10].

Proof: If $R(x, i) \geqslant 0$, then

$$\int_{t_0}^{t} v(\tau)\, i(\tau)\, d\tau = \int_{t_0}^{t} R(x(\tau), i(\tau))\, i^2(\tau)\, d\tau \geqslant 0, \quad \text{for all } t \geqslant t_0$$

and hence the one-port is passive. We prove the necessity part by contradiction. First, suppose that the one-port is passive and $R(x^*, i_0) < 0$ for some $i_0 \in \mathcal{R}$. Then by the continuity of the function R in $\mathcal{R}^{n+1}$, there exists an open neighborhood $B_0[(x^*, i_0), \delta]$ of $(x^*, i_0) \in \mathcal{R}^{n+1}$ in which $R(x, i) < 0$. Hence there exists an input waveform $i(\cdot)$ such that $i(t_0) = i_0$ and

$$\int_{t_0}^{t} v(\tau)\, i(\tau)\, d\tau < 0, \quad \text{for all } t \in (t_0, t_1)$$

[6] The same property obviously applies to the "dual" voltage-controlled case.

[7] This criterion can be easily extended to the time-varying case.

where t_1 depends on B_0 and $i(\cdot)$. But this contradicts the assumption that the one-port is passive and $R(x^*, i_0) \geqslant 0$ for any admissible $i_0 \in \mathcal{R}$.

Suppose next that $R(x_A, i_A) < 0$ for some $(x_A, i_A) \in \mathcal{R}^{n+1}$ where $x_A \neq x^*$. Then i_0 can be chosen such that we can draw a "connecting" arc Γ from (x^*, i_0) to (x_A, i_A) whose open arc (excluding the two end points) does not intersect the hyperplane $i = 0$. That is, if $i_A > 0$ choose $i_0 > 0$ and if $i_A < 0$ choose $i_0 < 0$. Since $R(x^*, i_0) \geqslant 0$ and $R(x_A, i_A) < 0$ by assumption, and since the function R is continuous in (x, i), there exists a point (x_B, i_B) on Γ at which $R(x_B, i_B) = 0$. However, this contradicts the assumption that $R(x, i) = 0$ only if $i = 0$, and hence $R(x, i) \geqslant 0$ for passivity to hold. ■

Property 2—No Energy Discharge Property

If a current-controlled memristive one-port satisfies the hypothesis of Property 1, then the instantaneous power entering the one-port is always nonnegative.

Proof: By hypothesis, $R(x, i) \geqslant 0$ for any admissible signal pair (v, i), and hence the instantaneous power entering the one-port (i.e., $p(t) = v(t)\, i(t)$) is always nonnegative.

Remark: Except for pathological cases, it is always possible to extract stored energy from a passive RLC one-port by simply connecting a load across it. However, for the case of a memristive one-port which satisfies Property 1, such energy discharge is never possible. To emphasize this unique property, we label it the "no energy discharge property."

Property 3—DC Characteristics

A time-invariant current-controlled memristive one-port under dc operation is equivalent to a time-invariant current-controlled nonlinear resistor if $f(x, I) = 0$ has a unique solution $x = X(I)$ such that for each value of $I \in \mathcal{R}$, the equilibrium point $x = X(I)$ is *globally asymptotically stable* [11].

Proof: Substituting $x = X(I)$ into the output equation in (2),[8] we obtain $V = R(X(I), I)\, I \triangleq \hat{V}(I)$. Since $X(I)$ is globally asymptotically stable, each value of dc input current I gives a stable, hence measurable, dc voltage V. Hence the function $\hat{V}(I)$ can be interpreted as the V–I curve of a time-invariant nonlinear resistor. ■

Remark: In practical analysis, Property 3 is still valid under low frequency periodic operation so long as the period of the excitation is much larger than the settling time of the associated transient response.

To illustrate the significance of Property 3, the dc characteristics of a thermistor with $\beta = 3460$ K, $\delta = 0.1$ mW/°C, $T_0 = 298$ K, and $R_0(T_0) = 8000\ \Omega$ are derived from (5) and (7) and are shown in Fig. 2 for $0 \leqslant I \leqslant 12.5$ mA. Notice that only the curve in the first quadrant is shown since the dc characteristic is symmetrical with respect to the origin. Such dc V–I characteristics are often supplied by thermistor manufacturers with the steady state temperature specified along the curve. Property 3 can now be used to interpret the use of this curve and its limitations; namely, *the dc thermistor V–I curve is useful only if the thermistor is to be operated under dc or slowly varying input signals*. Observe that the fact that a time-invariant memristive one-port under dc operation behaves just like a nonlinear resistor is one reason why so many memristive devices have been improperly identified as nonlinear resistors!

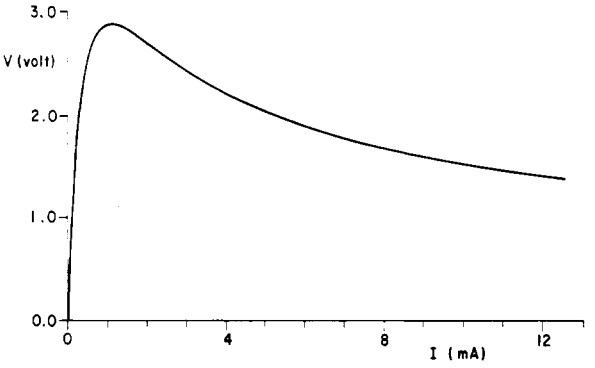

Fig. 2. The dc V–I curve of a typical thermistor.

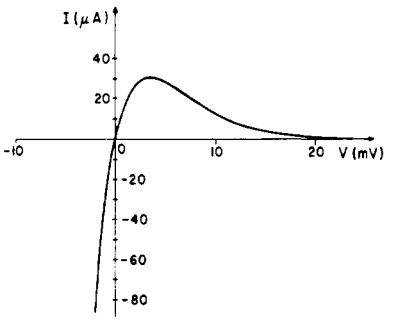

Fig. 3. The potassium channel dc characteristics.

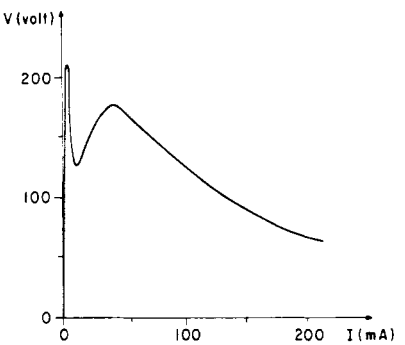

Fig. 4. The dc characteristics of a short neon tube.

The dc characteristic curve of the potassium channel (with $\bar{g}_K = 36$ m℧/cm^2 and $E_K = 12$ mV) of the Hodgkin–Huxley model described by (8) is shown in Fig. 3. Similarly, a typical dc V–I curve of discharge tubes is shown in Fig. 4. Again, only the first quadrant V–I curve is shown since it is symmetrical with respect to the origin. Observe that all these dc characteristic curves pass through the origin—as they should.

Property 4—Double-Valued Lissajous Figure Property

A current-controlled memristive one-port under periodic operation[9] with $i(t) = I \cos \omega t$ always gives rise to a v–i Lissajous figure whose voltage v is at most a double-valued function of i.

Proof: In the representation (2), the state equation has a unique periodic solution $x(t)$ for all $t \geqslant t_0$ for some initial state x_0, by assumption. Hence, for any value of the current $i \in [-I, I]$, there correspond at most two distinct values of v. ■

[8] Strictly speaking we are referring to the time-invariant version of representation (2).

[9] A one-port is said to be in *periodic operation* when its response is periodic with the same period as that of the input.

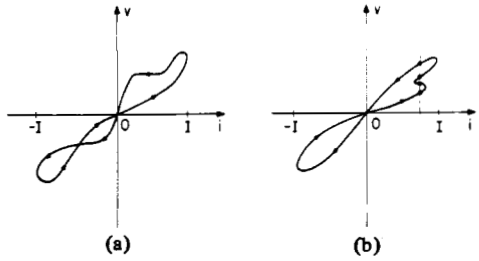

Fig. 5. Illustration of property 4. (a) Possible Lissajous figure. (b) Impossible Lissajous figure.

Remark: This property is illustrated in Fig. 5. Observe that the Lissajous figure in Fig. 5(b) cannot correspond to that of a current-controlled memristive one-port, because at $i = i_P$, there correspond more than two distinct values of v.

Property 5—Symmetric Lissajous Figure Property

If the readout map of a time-invariant current-controlled memristive one-port is such that $R(x, i) = R(x, -i)$, then the v-i Lissajous figure corresponding to the input current $i(t) = I \cos \omega t$ is *open* (i.e., not a closed loop) whenever the state $x(t)$ is periodic of the same period as that of the input $i(t)$ and is half-wave symmetric.[10] Moreover, it is *odd symmetric* with respect to the origin whenever the state $x(t)$ is periodic of the same period as that of $i(t)$ and is quarter-wave symmetric.

Proof: If both $x(t)$ and $i(t)$ are half-wave symmetric, then it follows from the output equation $v = R(x, i)i$ that

$$\begin{aligned} v\left(t+\frac{T}{2}\right) &= R\left(x\left(t+\frac{T}{2}\right), i\left(t+\frac{T}{2}\right)\right) i\left(t+\frac{T}{2}\right) \\ &= R\left(x\left(-t+\frac{T}{2}\right), i\left(-t+\frac{T}{2}\right)\right) i\left(-t+\frac{T}{2}\right) \\ &= v\left(-t+\frac{T}{2}\right), \quad \text{for all } t \in \left[0, \frac{T}{2}\right] \end{aligned}$$

where T is the period of both $x(t)$ and $i(t)$. Hence the v-i curve does not form a closed loop and is open. If $x(t)$ is quarter-wave symmetric, then since $i(t + T/4) = -i(-t + T/4)$ for all $t \in [0, T/4]$ when $i(t) = I \cos \omega t$, we obtain

$$\begin{aligned} v\left(t+\frac{T}{4}\right) &= R\left(x\left(t+\frac{T}{4}\right), i\left(t+\frac{T}{4}\right)\right) i\left(t+\frac{T}{4}\right) \\ &= -R\left(x\left(-t+\frac{T}{4}\right), i\left(-t+\frac{T}{4}\right)\right) i\left(-t+\frac{T}{4}\right) \\ &= -v\left(-t+\frac{T}{4}\right), \quad \text{for all } t \in \left[0, \frac{T}{4}\right]. \end{aligned}$$

Similarly, we can show that $v(t + 3T/4) = -v(-t + 3T/4)$ for all $t \in [0, T/4]$. Hence, the v-i curve is odd symmetric with respect to the origin. ■

Property 6—Limiting Linear Characteristics

If a time-invariant current-controlled memristive one-port described by (4) is bounded-input bounded-state (bibs) stable,[11] then under *periodic* operation it degenerates into a *linear time-invariant* resistor as the excitation frequency increases toward infinity.

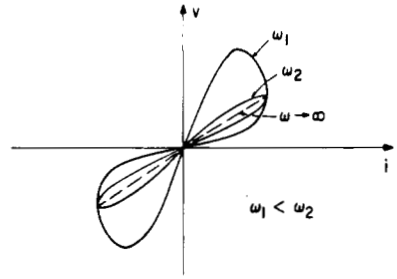

Fig. 6. Frequency response of Lissajous figures.

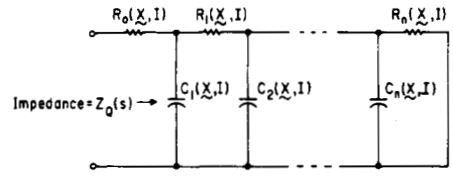

Fig. 7. The small-signal equivalent circuit.

Proof: It suffices to show that the state vector $x(t) \to x_0$ where x_0 is some constant vector in $\mathcal{R}^n$, as the excitation frequency $\omega \to \infty$. It follows from the bibs stability and the continuity of the function f in (4) that for any bounded input $i(t)$, $f(x, i)$ can be written as

$$f(x, i) = \alpha_0 + \sum_{\substack{k=-N \\ k\neq 0}}^{N} \exp(jk\omega t)\, \alpha_k \tag{11}$$

where N is some integer and the vectors α_0 and α_k belong to the space $\mathcal{C}^n$ of n-tuples of complex numbers. Note that the vectors α_0 and α_k are bounded. From (4) and (11) we obtain

$$\begin{aligned} x(t) &= x(t_0) + \int_{t_0}^{t} f(x(\tau), i(\tau))\, d\tau \\ &= x_0 + \int_{t_0}^{t} \left(\alpha_0 + \sum_{\substack{k=-N \\ k\neq 0}}^{N} \exp(jk\omega\tau)\, \alpha_k \right) d\tau \\ &= x_0 + \alpha_0(t - t_0) + \sum_{\substack{k=-N \\ k\neq 0}}^{N} \frac{\exp(jk\omega t) - \exp(jk\omega t_0)}{jk\omega} \alpha_k. \end{aligned} \tag{12}$$

Since $x(t)$ is periodic and bounded by assumption, (12) implies $\alpha_0 = 0$ and as $\omega \to \infty$, the state $x(t) \to x_0$. ■

Remark: When the memristive one-port is under periodic operation, different initial states x_0 will have to be chosen for different excitation frequencies. However, the state $x(t)$ still approaches some constant vector as the excitation frequency increases toward infinity. This property is illustrated in Fig. 6, where a family of Lissajous figures is shown shrinking to a straight line as $\omega \to \infty$.

Property 7—Small-Signal AC Characteristics

If a time-invariant current-controlled memristive one-port is globally asymptotically stable for all dc input current I, then its small-signal equivalent circuit about the dc operating point is as shown in Fig. 7.

[10] A periodic waveform $x(t)$ of period T is said to be *half-wave symmetric* if $x(t + kT/2) = x(-t + kT/2)$ for $k = 1, 2$ for all $t \in [0, T/2]$, and *quarter-wave symmetric* if $x(t + kT/4) = x(-t + kT/4)$ for $k = 1, 3$ for all $t \in [0, T/4]$.

[11] A dynamical system (4) is said to be bibs stable if for all t_0, for all initial states x_0 and for all bounded inputs $i_{[t_0,\infty)}$, the state trajectory $x(\cdot)$ is bounded.

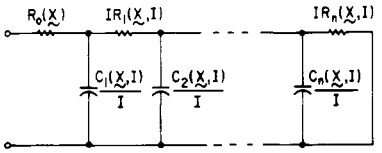

Fig. 8. The small-signal equivalent circuit for representation (4).

Proof: Let the input current $i(t)$ be such that

$$i(t) = I + \delta i(t), \text{ where } \sup_{t\in\mathcal{R}} |\delta i(t)| << |I| \tag{13}$$

and let a time-invariant current-controlled memristive one-port be characterized by

$$\dot{x} = f(x, i)$$
$$v = R(x, i)i \triangleq h(x, i). \tag{14}$$

If we linearize (14) about (X, I), where X is the solution of $f(x, I) = 0$, we obtain

$$\delta\dot{x} = \frac{\partial f(X,I)}{\partial x}\,\delta x + \frac{\partial f(X,I)}{\partial i}\,\delta i \triangleq A(X,I)\delta x + b(X,I)\delta i \tag{15}$$

$$\delta v = \frac{\partial h(X,I)}{\partial x}\,\delta x + \frac{\partial h(X,I)}{\partial i}\,\delta i \triangleq c(X,I)\delta x + d(X,I)\delta i \tag{16}$$

where

$$A(X,I) = \begin{bmatrix} \frac{\partial f_1(X,I)}{\partial x_1} & \frac{\partial f_1(X,I)}{\partial x_2} & \cdots & \frac{\partial f_1(X,I)}{\partial x_n} \\ \frac{\partial f_2(X,I)}{\partial x_1} & \frac{\partial f_2(X,I)}{\partial x_2} & \cdots & \frac{\partial f_2(X,I)}{\partial x_n} \\ \vdots & \vdots & & \vdots \\ \frac{\partial f_n(X,I)}{\partial x_1} & \frac{\partial f_n(X,I)}{\partial x_2} & \cdots & \frac{\partial f_n(X,I)}{\partial x_n} \end{bmatrix} \tag{17}$$

$$b(X,I) = \begin{bmatrix} \frac{\partial f_1(X,I)}{\partial i} & \frac{\partial f_2(X,I)}{\partial i} & \cdots & \frac{\partial f_n(X,I)}{\partial i} \end{bmatrix}^T \tag{18}$$

$$c(X,I) = \begin{bmatrix} \frac{\partial h(X,I)}{\partial x_1} & \frac{\partial h(X,I)}{\partial x_2} & \cdots & \frac{\partial h(X,I)}{\partial x_n} \end{bmatrix} \tag{19}$$

and

$$d(X,I) = \frac{\partial h(X,I)}{\partial i}. \tag{20}$$

Taking Laplace transform of both sides of (15) and (16) with $\delta x(0) = 0$, we obtain

$$s\,\Delta X(s) = A(X,I)\,\Delta X(s) + b(X,I)\,\Delta I(s) \tag{21}$$

$$\Delta V(s) = c(X,I)\,\Delta X(s) + d(X,I)\,\Delta I(s). \tag{22}$$

Solving for $\Delta X(s)$ from (21), we obtain

$$\Delta X(s) = [s1 - A(X,I)]^{-1}\, b(X,I)\,\Delta I(s) \tag{23}$$

where 1 denotes an identity matrix of order n.

Substituting (23) into (22), we obtain

$$\Delta V(s) = \{c(X,I)[s1 - A(X,I)]^{-1}\, b(X,I) + d(X,I)\}\Delta I(s). \tag{24}$$

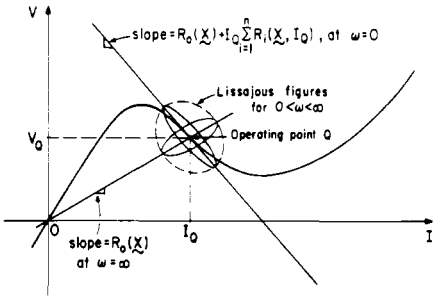

Fig. 9. The small-signal Lissajous figures.

It follows from (24) that the *small-signal impedance* for a time-invariant current-controlled memristive one-port is given by

$$Z_Q(s) \triangleq \frac{\Delta V(s)}{\Delta I(s)} = d(X,I) + \frac{\beta_1 s^{n-1} + \beta_2 s^{n-2} + \cdots + \beta_{n-1} s + \beta_n}{s^n + \alpha_1 s^{n-1} + \alpha_2 s^{n-2} + \cdots + \alpha_{n-1} s + \alpha_n} \tag{25}$$

where α_i, β_i are functions of $(X, I) \in \mathcal{R}^n \times \mathcal{R}$. Equation (25) can be rewritten into the form of a continued fraction expansion

$$Z_Q(s) = d(X,I) + \cfrac{1}{sC_1 + \cfrac{1}{R_1 + \cfrac{1}{sC_2 + \cfrac{1}{\ddots + \cfrac{1}{sC_n + \cfrac{1}{R_n}}}}}} \tag{26}$$

where again C_i and R_i are functions of (X, I). The circuit in Fig. 7 follows from (26) upon setting $R_0(X, I) = d(X, I)$. ■

Remark 1: For the case of time-invariant current-controlled memristive one-port described by (4), the associated small-signal equivalent circuit is as shown in Fig. 8. Observe that Fig. 8 is obtained from Fig. 7 upon replacing $R_0(X, I)$ by $R_0(X)$, $R_i(X, I)$ by $I\,R_i(X, I)$ and $C_i(X, I)$ by $C_i(X, I)/I$. When the biasing current $I = 0$, the small-signal input impedance $Z_Q(s)$ reduces to that of a linear resistor $R_0(X)$ and is therefore purely dissipative for $R_0(X) > 0$.

Remark 2: As the excitation frequency of the small signal $\delta i(t)$ approaches zero, the small-signal impedance $Z_Q(s)$ in Fig. 8 degenerates into

$$Z_Q(s) = R_0(X) + I_Q \sum_{i=1}^{n} R_i(X, I_Q). \tag{27}$$

The small-signal impedance in (27) corresponds to the slope of the dc V-I curve at $I = I_Q$. The value $R_0(X)$ represents the dc resistance at $I = I_Q$ and is equal to the small-signal impedance $Z_Q(s)$ as the excitation frequency increases toward infinity.

The frequency dependence of the small-signal Lissajous figures about the operating point $I = I_Q$ is depicted in Fig. 9.

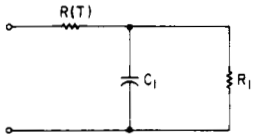

$$C_1 = \frac{C}{2\alpha P R(T)} \triangleq \hat{C}_1(T, I)$$

$$R_1 = \frac{2\alpha P R(T)}{\beta - \alpha P} \triangleq \hat{R}_1(T, I)$$

where $\alpha \triangleq -\frac{\beta}{T^2} < 0$, $P \triangleq VI = R(T)I^2$

Fig. 10. The small-signal equivalent circuit for the thermistor.

This behavior has been observed in many physical devices and systems, including thermistors and ionic systems[12] [12].

Remark 3: The small-signal equivalent circuits for the thermistor and the potassium channel of the Hodgkin–Huxley model are shown in Figs. 10 and 11. In Fig. 10, $C_1 \triangleq C/2\alpha PR(T)$, where $\alpha \triangleq -\beta/T^2 < 0$ and $P = VI$. Since C_1 is negative, the thermistor is inductive under small-signal operation. In Fig. 11, the small-signal admittance $Y_Q(s)$ of the potassium channel can be shown to be inductive for $V > 0$ and capacitive for $V < 0$.

Property 8–Local Passivity Criteria

A first-order time-invariant current-controlled memristive one-port described by (4) is *locally passive* with respect to an operating point $I = I_Q$ if and only if,

$$\text{i)} \quad \frac{\partial f(X, I)}{\partial x} \leqslant 0$$

$$\text{ii) } R(X) \geqslant 0 \text{ and } \begin{cases} R(X) \geqslant \dfrac{\dfrac{\partial f(X,I)}{\partial i}\dfrac{\partial R(X)}{\partial x} I}{\dfrac{\partial f(X,I)}{\partial x}}, \\ \qquad \text{when } \dfrac{\partial f(X,I)}{\partial x} \neq 0 \\ \dfrac{\partial f(X,I)}{\partial i}\dfrac{\partial R(X)}{\partial x} I > 0, \\ \qquad \text{when } \dfrac{\partial f(X,I)}{\partial x} = 0. \end{cases} \quad (28)$$

Proof: The small-signal impedance of a first-order time-invariant current-controlled memristive one-port described by (4) is

$$Z_Q(s) = R(X) + \frac{\dfrac{\partial f(X,I)}{\partial i}\dfrac{\partial R(X)}{\partial x} I}{s - \dfrac{\partial f(X,I)}{\partial x}}. \quad (29)$$

In order for $Z_Q(s)$ to be the impedance of a passive one-port, it is necessary and sufficient that $Z_Q(s)$ be positive real. The conditions given in (28) follow directly from the well-known pr criteria [13].

[12]Mauro [12] was so perplexed and mystified by these unconventional behaviors that he collectively referred to these elements as an anomalous impedance!

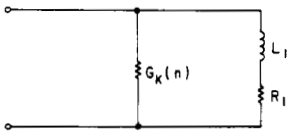

$$G_K(n) = \bar{g}_K n^4$$

$$L_1 = \frac{1}{4\bar{g}_K n^4 V\left[\frac{1-n}{n}\frac{\partial \alpha_n(V)}{\partial v} - \frac{\partial \beta_n(V)}{\partial v}\right]} \triangleq \hat{L}_1(n, V)$$

$$R_1 = \frac{\alpha_n(V) + \beta_n(V)}{4\bar{g}_K n^4 V\left[\frac{1-n}{n}\frac{\partial \alpha_n(V)}{\partial v} - \frac{\partial \beta_n(V)}{\partial v}\right]} \triangleq \hat{R}_1(n, V)$$

where $\alpha_n(v) = \dfrac{0.01(v + E_K + 10)}{\exp[(v + E_K + 10)/10] - 1}$

$$\beta_n(v) = 0.125 \exp\left(\frac{v + E_K}{80}\right)$$

Fig. 11. The small-signal equivalent circuit for the potassium channel of the Hodgkin–Huxley model.

Remark: The potassium channel of the Hodgkin–Huxley model violates the second criterion (with i replaced by v) at $V = 10$ mV and hence is locally active at this operating point. This is verified by the fact that in Fig. 3 the slope of the V–I curve at $V = 10$ mV is negative. For the case of the thermistor described by (5) and (7), the second criterion is also violated at $I = 1.5$ mA, and hence the thermistor is also locally active at this operating point. Observe that the slope of the V–I curve at $I = 1.5$ mA is negative, which is consistent with the local activity of the thermistor.

General Remarks on the Generic Properties

The properties derived above can be used not only to identify those memristive devices and systems which have so far eluded a correct identification, but also to suggest potential applications. For example, the local activity of the thermistor and the potassium channel of the Hodgkin–Huxley model has important practical significance. Indeed, the two-thermistor circuit shown in Fig. 12 has been designed to function as an ultralow-frequency oscillator by biasing the thermistors in their locally active regions [14]. It is also well known that the Hodgkin–Huxley model is locally active and hence is capable of firing nerve impulses. Many more examples abound which possess the generic properties of memristive systems [12].

There are good reasons to believe that many physical and biological systems should be modeled as memristive one-ports. To identify such devices and systems, we look for the following properties of the one-port $\mathcal{N}$ under investigation:

1) The dc characteristic curve of $\mathcal{N}$ passes through the origin.
2) The v–i Lissajous figures corresponding to any periodic excitation having a zero mean value always pass through the origin.
3) The one-port $\mathcal{N}$ behaves as a linear resistor as the excitation frequency ω increases toward infinity.[13]
4) For a memristive one-port $\mathcal{N}$ which admits the representation (4), its small-signal impedance degenerates into a pure resistor under zero bias, but becomes either inductive or capacitive depending on the operating point.

[13]If a one-port is not bibs stable, then it is possible that the memristive one-port does not behave as a linear resistor as ω increases toward infinity. This situation, however, is highly pathological.

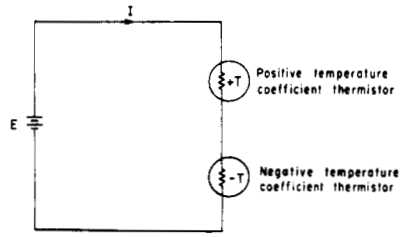

Fig. 12. A two-thermistor circuit which functions as an ultralow-frequency oscillator.

5) The order of the small-signal impedance (or admittance) is invariant with respect to the dc biasing current (or voltage).

III. A Canonical Model for Memristive One-Ports

Once a device or system has been identified as memristive, the next task will be to find a suitable mathematical model describing its behavior. Our objective in this section is to present a canonical model which will correctly mimic the steady state response of memristive one-ports to the following class of input "testing signals":

1) DC or slowly varying waveforms.
2) Sinusoidal signals of arbitrary amplitudes and frequencies.
3) Sinusoidal signals of arbitrary amplitudes and frequencies superimposed on top of a dc bias.

We will denote the above class of input testing signals by

$$\mathcal{U} \triangleq \{u(t) \triangleq A_0 + A \cos \omega t \mid (t, \omega) \in \mathcal{R} \times [1, \infty)\} \quad (30)$$

where $(A_0, A) \in \mathcal{R} \times \mathcal{R}_+$, $\mathcal{R}_+ \triangleq [0, \infty)$. The constants A_0 and A represent the dc component and the amplitude of the sinusoidal component of the input testing signals, respectively. Observe that the lower bound on the frequency range in (30) is not a stringent restriction since in practical applications we can always normalize any given set of nonzero frequencies so that the lowest frequency becomes unity. In (30), the value of A is set equal to zero for dc operation, while the value of A_0 is set equal to zero for sinusoidal excitations. When the one-port is operating in the small signal mode, A will be set equal to a small positive number and A_0 will be set equal to some biasing value. These testing signals are chosen mainly because they are the ones most commonly used in laboratory tests. Although our model is derived to yield exact simulations only for these testing signals, the fact that our model also possesses all the *generic properties* presented in the preceding section suggests that it should also give reasonably realistic simulations for arbitrary testing signals.

Our main assumption in the following derivation is that the system response $y(t)$ tends to a unique steady state for each input $u(t) \in \mathcal{U}$ such that the function $\rho(t) \triangleq y(t)/u(t)$ tends to a periodic waveform of the same period as that of the input $u(t)$ in steady state.[14] Observe that each input testing signal $u(t) \in \mathcal{U}$ is uniquely specified by three numbers, namely; A_0, A, and ω. Hence for each combination of $\{A_0, A, \omega\}$, there corresponds a unique $\rho(t)$. In other words, $\rho(t)$ is actually a function of A_0, A, and ω and to be precise, we may denote it by $\rho(t; A_0, A, \omega)$. Let the *steady-state component* of $\rho(t)$ be denoted by $\rho_s(t)$. Since the function $\rho_s(t)$ is periodic of the same period as that of input $u(t)$, by assumption, it admits the following Fourier series representation:

$$\rho_s(t) = a_0(A_0, A, \omega) + \sum_{k=1}^{N} \{a_k(A_0, A, \omega) \cos k\omega t + b_k(A_0, A, \omega) \sin k\omega t\} \quad (31)$$

where the integer N is an arbitrary number which is determined by $\rho_s(t)$.[15] The Fourier coefficients in (31) are determined by

$$a_0(A_0, A, \omega) = \frac{\omega}{2\pi} \int_0^{2\pi/\omega} \rho_s(\tau; A_0, A, \omega)\, d\tau \quad (32)$$

$$a_k(A_0, A, \omega) = \frac{\omega}{\pi} \int_0^{2\pi/\omega} \rho_s(\tau; A_0, A, \omega) \cos k\omega\tau\, d\tau \quad (33)$$

and

$$b_k(A_0, A, \omega) = \frac{\omega}{\pi} \int_0^{2\pi/\omega} \rho_s(\tau; A_0, A, \omega) \sin k\omega\tau\, d\tau. \quad (34)$$

These coefficients are assumed to be continuous functions of A_0 and A in the mean-square sense, and square-integrable functions of ω; namely: 1) for each $\epsilon > 0$ and for each $(\hat{A}_0, \hat{A}) \in \mathcal{R} \times \mathcal{R}_+$, there exists a neighborhood N_δ of $(\hat{A}_0, \hat{A})$ such that

$$\|a_0(A_0, A, \omega) - a_0(\hat{A}_0, \hat{A}, \omega)\|_{L^2} < \epsilon \quad (35)$$

$$\|a_k(A_0, A, \omega) - a_k(\hat{A}_0, \hat{A}, \omega)\|_{L^2} < \epsilon \quad (36)$$

and

$$\|b_k(A_0, A, \omega) - b_k(\hat{A}_0, \hat{A}, \omega)\|_{L^2} < \epsilon \quad (37)$$

for all $(A_0, A) \in N_\delta$, where L^2 denotes the space of square-integrable functions. 2) $a_0(A_0, A, \cdot)$, $a_k(A_0, A, \cdot)$ and $b_k(A_0, A, \cdot)$ are square-integrable functions of ω, i.e., they belong to $L^2_{(0,\infty)}$.

Before we present a canonical state-space model for memristive one-ports which satisfies the preceding assumptions,[16] we will introduce two families of complete orthonormal functions in $L^2_{[1/k,\infty)}$. These functions will allow a unique decomposition of the Fourier coefficients into the product between a *frequency-dependent component* and a *frequency-independent component* which depends only on A_0 and A of the input $u(t) \in \mathcal{U}$. The two families of complete orthonormal functions are defined by [15]:

$$\mathcal{A}_k \triangleq \left\{ a_{kl}(\omega) \triangleq k^{1/2} \sum_{m=1}^{l} \frac{\alpha_{lm}}{(k\omega)^{2m}} \;\middle|\; \omega \in \left[\frac{1}{k}, \infty\right),\ l \in \mathcal{I} \right\} \quad (38)$$

$$\mathcal{B}_k \triangleq \left\{ b_{kl}(\omega) \triangleq k^{1/2} \sum_{m=1}^{l} \frac{\beta_{lm}}{(k\omega)^{2m}} \;\middle|\; \omega \in \left[\frac{1}{k}, \infty\right),\ l \in \mathcal{I} \right\} \quad (39)$$

[14] The frequency of $\rho(t)$ in steady state may be a harmonic of the input frequency, but neither subharmonics nor incommensurate frequencies are allowed in $\rho(t)$.

[15] In most practical cases the integer N is a finite number. If it is not a finite number, then we will approximate $\rho_s(t)$ by a finite Fourier series expansion up to the Nth harmonic term and model the approximated waveform.

[16] These assumptions can be relaxed such that whenever there is a Fourier coefficient containing terms that are not functions of the excitation frequency ω, then the ω-dependent terms are square-integrable functions of ω and the ω-independent terms are continuous functions of (A_0, A). The model presented is also valid under these relaxed assumptions.

where $\mathcal{I}$ denotes the set of natural numbers and α_{lm} and β_{lm} are constants defined by

$$\alpha_{lm} \triangleq (4l-1)^{1/2} \frac{\prod_{n=1}^{l-1} \{2(m+n)-1\}}{\prod_{\substack{n=1 \\ n\neq m}}^{l} 2(m-n)}, \quad m \leq l \quad (40)$$

$$\beta_{lm} \triangleq (4l+1)^{1/2} \frac{\prod_{n=1}^{l-1} \{2(m+n)+1\}}{\prod_{\substack{n=1 \\ n\neq m}}^{l} 2(m-n)}, \quad m \leq l. \quad (41)$$

The families $\mathcal{A}_k$ and $\mathcal{B}_k$ will be used shortly to construct the readout map of our state-space model. To model the steady state response of memristive one-ports subject to the input testing signals $u(t) \in \mathcal{U}$, we propose the following.

Canonical State-Space Model Representation

State equation[17]:

$$\begin{aligned} \dot{x}_1 &= -a(t)\, x_1 + b(t)\, u \\ \dot{x}_2 &= -x_1 + u \\ \dot{x}_3 &= p(u - x_1 - x_3) \\ \dot{x}_4 &= p(-x_2 - x_4) \end{aligned} \quad (42a)$$

where $x_0 \triangleq [x_1(0), x_2(0), x_3(0), x_4(0)]^T = 0$.

Output equation:

$$y = g(x_1, x_2, x_3, x_4, u)u \quad (42b)$$

where

$$a(t) = \frac{1 - e^{-Kt}}{t + (1/K)\, e^{-Kt}}, \quad b(t) = \frac{1}{t + (1/K)\, e^{-Kt}}, \quad K \gg 1 \quad (42c)$$

and $p(\cdot)$ is a monotonically increasing nonlinear function whose graph is similar to the diode characteristic curve. The nonlinear map $g(\cdot)$ in the output equation (42b) is defined by

$$\begin{aligned} g(x_1, x_2, x_3, x_4, u) \triangleq \sum_{l=1}^{M} \zeta_{0l}(x_1, x_3)\, a_{1l}\left(\left(1+\frac{\pi}{2}\right)\frac{x_3}{x_4}\right) \\ + \sum_{k=1}^{N}\left\{\left[\sum_{l=1}^{M} \gamma_{kl}(x_1, x_3)\, a_{kl}\left(\left(1+\frac{\pi}{2}\right)\cdot\frac{x_3}{x_4}\right)\right] T_k\left(\frac{u-x_1}{x_3}\right) + \left[\sum_{l=1}^{M} \delta_{kl}(x_1, x_3)\cdot b_{kl}\left(\left(1+\frac{\pi}{2}\right)\frac{x_3}{x_4}\right)\right] \cdot \left(\left(1+\frac{\pi}{2}\right)\frac{x_2}{x_4} + \frac{\pi}{2}\right) U_{k-1}\left(\frac{u-x_1}{x_3}\right)\right\} \end{aligned} \quad (43)$$

where M is an integer, and $\zeta_{0l}(\cdot)$, $\gamma_{kl}(\cdot)$ and $\delta_{kl}(\cdot)$ are *scalar nonlinear functions* of x_1 and x_3 which are identified via the following *Fourier coefficient expansions*:

$$\zeta_{0l}(A_0, A) = \int_1^{\infty} a_0(A_0, A, \omega)\, a_{1l}(\omega)\, d\omega \quad (44)$$

$$\gamma_{kl}(A_0, A) = \int_{1/k}^{\infty} a_k(A_0, A, \omega)\, a_{kl}(\omega)\, d\omega \quad (45)$$

$$\delta_{kl}(A_0, A) = \int_{1/k}^{\infty} b_k(A_0, A, \omega)\, b_{kl}(\omega)\, d\omega. \quad (46)$$

The functions $a_0(\cdot)$, $a_k(\cdot)$ and $b_k(\cdot)$ in these equations are themselves Fourier coefficients of $\rho_s(t)$ defined in (31) while $a_{kl}(\cdot)$ and $b_{kl}(\cdot)$ are *basis functions* defined in (38) and (39). In (43), N is a fixed integer defined via (31) and $T_k(\cdot)$, $U_k(\cdot)$ are the Chebyshev polynomial functions of the first and second kind, respectively; namely [16],

$$T_k(z) \triangleq \frac{k}{2} \sum_{j=0}^{[k/2]} (-1)^j \frac{(k-j-1)!}{j!\,(k-2j)!} (2z)^{k-2j} \quad (47)$$

$$U_k(z) \triangleq \sum_{j=0}^{[k/2]} (-1)^j \frac{(k-j)!}{j!\,(k-2j)!} (2z)^{k-2j} \quad (48)$$

where $[k/2]$ denotes largest integer less than or equal to $k/2$.

Observe that in spite of the seemingly complicated algebraic structure of the preceding canonical model, *the only model parameter and model functions that need to be identified are the integer M and $(2N+1)M$ nonlinear functions, $\zeta_{0l}(\cdot)$, $\gamma_{kl}(\cdot)$ and $\delta_{kl}(\cdot)$, and the nonlinear function $p(\cdot)$.* As mentioned earlier the nonlinear function $p(\cdot)$ may be any strictly monotonically increasing Lipschitz continuous function whose graph is similar to the diode characteristic curve. However, for simplicity, we will choose $p(\cdot)$ to be a *piecewise linear* function defined by [15]

$$p(e) \triangleq \alpha e + (1/\alpha - \alpha) r(e) \quad (49)$$

where $\alpha \in (0,1)$ and $r(\cdot)$ is a unit ramp function, i.e.,

$$r(e) \triangleq \begin{cases} e, & \text{for } e \geq 0 \\ 0, & \text{for } e < 0. \end{cases} \quad (50)$$

Notice from (49) that the nonlinear function $p(\cdot)$ is uniquely specified by the parameter $\alpha \in (0, 1)$. Hence, only the value of α need be identified.

We will present an algorithm that will determine the model parameters M and α and the $(2N+1)M$ nonlinear functions. Before we state the algorithm let us first define the following *stop rule*. Given any set of input testing signals $\mathcal{U}_D \triangleq \{u_{ijk}(t) \triangleq A_{0i} + A_j \cos \omega_k t\}$, where the subscripts i, j, k range from 1 to N_{A_0}, N_A, N_ω, respectively, the *performance index* of the model with respect to these testing signals is defined to be[18]

$$\eta \triangleq \sum_{i=1}^{N_{A_0}} \sum_{j=1}^{N_A} \sum_{k=1}^{N_\omega} \frac{\omega_k}{2\pi} \int_0^{2\pi/\omega_k} |\rho_s(\tau; u_{ijk}) - \hat{\rho}_s(\tau; u_{ijk})|^2\, d\tau \quad (51)$$

where $\rho_s(t; u_{ijk})$ denotes the steady-state component of $\rho(t)$ in the original system and $\hat{\rho}_s(t; u_{ijk})$ denotes the steady-state component of $\hat{\rho}(t)$ in the model subject to the input

[17] Equation (42a) may be replaced by a *time-invariant* system of state equations upon introducing two additional state variables. In particular, if we choose $\dot{y}_1 = y_2$, $\dot{y}_2 = K(1 - y_2)$ with initial state $y_1(0) = 1/K$, $y_2(0) = 0$, then $a(t) = y_2/y_1$ and $b(t) = 1/y_1$.

[18] We are assuming without loss of generality that the time instant at which both $\rho(t)$ and $\hat{\rho}(t)$ attain steady state has been set to zero. Hence, by this assumption, $\rho_s(t)$ and $\hat{\rho}_s(t)$ are periodic on $\mathcal{R}_+$ after an appropriate time translation.

$u_{ijk}(t) \in \mathfrak{U}_D$. Another *error index* to be used is[19]

$$\epsilon_M \triangleq \sum_{i=1}^{N_{A_0}} \sum_{j=1}^{N_A} \sum_{k=1}^{N_\omega} \left| a_0(A_{0i}, A_j, \omega_k) - \sum_{l=1}^{M} \zeta_{0l}(A_{0i}, A_j)\, a_{1l}(\omega_k) \right|^2 + \sum_{n=1}^{N} \left\{ \left| a_n(A_{0i}, A_j, \omega_k) - \sum_{l=1}^{M} \gamma_{nl}(A_{0i}, A_j)\, a_{nl}(\omega_k) \right|^2 + \left| b_n(A_{0i}, A_j, \omega_k) - \sum_{l=1}^{M} \delta_{nl}(A_{0i}, A_j)\, b_{nl}(\omega_k) \right|^2 \right\} \quad (52)$$

where $a_0(\cdot)$, $a_n(\cdot)$, and $b_n(\cdot)$ are the Fourier coefficients of $\rho_s(t; u_{ijk})$ defined in (31)–(34), and $a_{nl}(\cdot)$, $b_{nl}(\cdot)$ are defined in (38) and (39). The error ϵ_M is a function of the integer M and the nonlinear functions $\zeta_{0l}(\cdot)$, $\delta_{nl}(\cdot)$. To initiate the algorithm, we need to prescribe an *upper bound* $\eta_{\max} \in (0, 1)$ for the performance index η. We also need to assume an initial guess on the iterative parameter $\alpha \in (0, 1)$.

Model Parameter and Function Identification Algorithm

Step 0: Select an $\alpha \in (0,1)$, and $\eta_{\max} \in (0, 1)$. Set $l = 1$.
Step 1: Compute $\zeta_{0l}(A_{0i}, A_j)$, $\gamma_{nl}(A_{0i}, A_j)$ and $\delta_{nl}(A_{0i}, A_j)$ from (44)–(46) for $n = 1, 2, \cdots, N$ for each i, j ranging from 1 to N_{A_0} and N_A, respectively.
Step 2: Set $M = l$ and compute ϵ_M using (52).
Step 3: If $\epsilon_M > \eta_{\max}/3$ set $l = l + 1$ and go to Step 1.
Step 4: Compute the performance index η using (51).
Step 5: If $\eta > \eta_{\max}$, set $\alpha = \alpha/2$ and go to Step 4. Otherwise stop.

The convergence is guaranteed by the following theorem.

Main Theorem

If the Fourier series representation of $a_0(A_0, A, \cdot)$ *relative to the basis functions in* $\mathfrak{A}_1$, $a_k(A_0, A, \cdot)$ *relative to the basis functions in* $\mathfrak{A}_k$, and $b_k(A_0, A, \cdot)$ *relative to the basis functions in* $\mathfrak{B}_k$ converge uniformly over the set of testing signal components $\{(A_{0i}, A_j)\}$ for i, j ranging from 1 to N_{A_0} and N_A, respectively, and for $k = 1, 2, \cdots, N$, then for each $\eta_{\max} > 0$ the preceding algorithm terminates in a finite number of iterations.

Proof: For each (A_0, A), the scalars $\zeta_{0l}(A_0, A)$, $\gamma_{kl}(A_0, A)$, and $\delta_{kl}(A_0, A)$ as defined by (44)–(46) are the Fourier coefficients of $a_0(A_0, A, \cdot)$, $a_k(A_0, A, \cdot)$ and $b_k(A_0, A, \cdot)$ relative to the basis functions in the complete orthonormal sets $\mathfrak{A}_1$, $\mathfrak{A}_k$, and $\mathfrak{B}_k$. Hence by the uniform convergence hypothesis, there exists a finite integer M such that ϵ_M defined by (52) is less than or equal to $\eta_{\max}/3$ for any $\eta_{\max} > 0$, i.e.,

$$\epsilon_M \leqslant \eta_{\max}/3. \quad (53)$$

From Lemma A-1 of the Appendix A, $\zeta_{0l}(A_{0i}, A_j)$, $\gamma_{kl}(A_{0i}, A_j)$ and $\delta_{kl}(A_{0i}, A_j)$ are continuous functions of (A_{0i}, A_j). From Theorem A-1 in the Appendix A, there exists a $\delta \in (0, 1)$ such that for any $\alpha \in (0, \delta)$, the steady state solution of the state equation (42a) yields arbitrarily close approximations $\hat{A}_{0i}$, $\hat{A}_j$, and $\hat{\omega}_k$ to A_{0i}, A_j, and ω_k, respectively. Also by the continuity of the Chebyshev polynomials $T_k(\cdot)$ and $U_k(\cdot)$ of the first and second kind as defined in (47) and (48), $\cos n\omega t$ and $\sin n\omega t$ can be approximated arbitrarily closely in steady state by

$$T_n\left(\frac{u - x_1}{x_3}\right) \quad \text{and} \quad \left(\left(1 + \frac{\pi}{2}\right)\frac{x_2}{x_4} + \frac{\pi}{2}\right) U_{n-1}\left(\frac{u - x_1}{x_3}\right)$$

where $u \in \mathfrak{U}$, respectively. For convenience, we denote these approximating functions by

$$C_n(t) \triangleq T_n\left(\frac{u(t) - x_1(t)}{x_3(t)}\right)$$

and

$$S_n(t) \triangleq \left(\left(1 + \frac{\pi}{2}\right)\frac{x_2(t)}{x_4(t)} + \frac{\pi}{2}\right) U_{n-1}\left(\frac{u(t) - x_1(t)}{x_3(t)}\right).$$

From (31), (43), and (51), we obtain

$$\eta \triangleq \sum_{i=1}^{N_{A_0}} \sum_{j=1}^{N_A} \sum_{k=1}^{N_\omega} \frac{\omega_k}{2\pi} \int_0^{2\pi/\omega_k} \Bigg| a_0(A_{0i}, A_j, \omega_k) + \sum_{n=1}^{N} \Big\{ a_n(A_{0i}, A_j, \omega_k) \cos n\omega_k \tau + b_n(A_{0i}, A_j, \omega_k) \sin n\omega_k \tau \Big\} - \sum_{l=1}^{M} \zeta_{0l}(\hat{A}_{0i}, \hat{A}_j)\, a_{1l}(\hat{\omega}_k) - \sum_{n=1}^{N} \left\{ \left[\sum_{l=1}^{M} \gamma_{nl}(\hat{A}_{0i}, \hat{A}_j)\, a_{nl}(\hat{\omega}_k) \right] C_n(\tau) + \left[\sum_{l=1}^{M} \delta_{nl}(\hat{A}_{0i}, \hat{A}_j)\, b_{nl}(\hat{\omega}_k) \right] S_n(\tau) \right\} \Bigg|^2 d\tau. \quad (54)$$

It follows from (54) and the triangular inequality that

$$\eta \leqslant \left\{ \sum_{i=1}^{N_{A_0}} \sum_{j=1}^{N_A} \sum_{k=1}^{N_\omega} \left[\left| a_0(A_{0i}, A_j, \omega_k) - \sum_{l=1}^{M} \zeta_{0l}(A_{0i}, A_j)\, a_{1l}(\omega_k) \right|^2 + \sum_{n=1}^{N} \left(\left| a_n(A_{0i}, A_j, \omega_k) - \sum_{l=1}^{M} \gamma_{nl}(A_{0i}, A_j)\, a_{nl}(\omega_k) \right|^2 + \left| b_n(A_{0i}, A_j, \omega_k) - \sum_{l=1}^{M} \delta_{nl}(A_{0i}, A_j)\, b_{nl}(\omega_k) \right|^2 \right) \right] \right\}$$

$$+ \left\{ \sum_{i=1}^{N_{A_0}} \sum_{j=1}^{N_A} \sum_{k=1}^{N_\omega} \left[\sum_{l=1}^{M} |\zeta_{0l}(A_{0i}, A_j)\, a_{1l}(\omega_k) - \zeta_{0l}(\hat{A}_{0i}, \hat{A}_j)\, a_{1l}(\hat{\omega}_k)|^2 + \sum_{n=1}^{N} \left(|\gamma_{nl}(A_{0i}, A_j)\, a_{nl}(\omega_k) - \gamma_{nl}(\hat{A}_{0i}, \hat{A}_j)\, a_{nl}(\hat{\omega}_k)|^2 + |\delta_{nl}(A_{0i}, A_j)\, b_{nl}(\omega_k) - \delta_{nl}(\hat{A}_{0i}, \hat{A}_j)\, b_{nl}(\hat{\omega}_k)|^2 \right) \right] \right\}$$

$$+ \left\{ \sum_{i=1}^{N_{A_0}} \sum_{j=1}^{N_A} \sum_{k=1}^{N_\omega} \frac{\omega_k}{2\pi} \int_0^{2\pi/\omega_k} \left(|\gamma_{nl}(\hat{A}_{0i}, \hat{A}_j)\, a_{nl}(\hat{\omega}_k)|^2 \cdot |\epsilon_{c_n}(\tau)|^2 + |\delta_{nl}(\hat{A}_{0i}, \hat{A}_j)\, b_{nl}(\hat{\omega}_k)|^2 \cdot |\epsilon_{s_n}(\tau)|^2 \right) d\tau \right\}$$

$$\triangleq E_1 + E_2 + E_3 \quad (55)$$

[19] The second error index ϵ_M is used to ensure that the model parameter M and the nonlinear model functions $\zeta_{0l}(\cdot)$, $\gamma_{nl}(\cdot)$, and $\delta_{nl}(\cdot)$ are determined properly so that the Fourier coefficients $a_0(\cdot)$, $a_n(\cdot)$ and $b_n(\cdot)$ can be approximated closely for the given components A_{0i}, A_j, and ω_k.

where $\epsilon_{c_n}(t)$, $\epsilon_{s_n}(t)$ are defined by

$$C_n(t) = \cos n\omega t + \epsilon_{c_n}(t) \tag{56}$$

$$S_n(t) = \sin n\omega t + \epsilon_{s_n}(t). \tag{57}$$

Hence, it follows from (52) and Step 3 of the algorithm that

$$E_1 \leqslant \eta_{\max}/3. \tag{58}$$

Moreover, since $\zeta_{0l}(\cdot)$, $\gamma_{nl}(\cdot)$, $\delta_{nl}(\cdot)$; $a_{nl}(\cdot)$ and $b_{nl}(\cdot)$ are continuous, it follows from Theorem A.1 in Appendix A that there exists a $\delta_1 \in (0, 1)$ such that for any $\alpha \in (0, \delta_1)$

$$E_2 \leqslant \eta_{\max}/6. \tag{59}$$

Since the Fourier coefficients of $\rho_s(t)$ are by assumption bounded for any input testing signal $u_{ijk}(t)$, there exist a $\delta_2 \in (0, 1)$ such that for any $\alpha \in (0, \delta_2)$

$$E_3 \leqslant \eta_{\max}/6. \tag{60}$$

Hence, for any $\alpha \in (0, \bar{\delta})$, where $\bar{\delta} = \min\{\delta_1, \delta_2\}$, we obtain from (55) and (58)–(60) the inequality

$$\eta \leqslant \eta_{\max}.$$

The preceding model is *canonical* in the sense that given any memristive one-port satisfying the technical assumptions described earlier, we can construct a dynamical system model having the same structure given in (42). The state equation (42a) is *fixed*—independent of the device or system being modeled—except for the parameter α defining the nonlinear function $p(\cdot)$ which has to be chosen properly so that *the time constant of the model is much smaller than the period of the input signals*.[20] To illustrate the implementation and the validity of the preceding algorithm, we present next a *hypothetical* memristive system and then derive its associated model. We choose a hypothetical example rather than a real device in order that the input–output signal pairs can be generated accurately on a digital computer.

Example:

Let $\mathfrak{N}$ be a fifth-order memristive one-port characterized by

$$\begin{aligned}
\dot{x}_1 &= -2x_1 + 2x_2\, i \\
\dot{x}_2 &= -x_2 + i \\
\dot{x}_3 &= -4x_3 + 2x_4\, i^2 \\
\dot{x}_4 &= -2x_4 + i^2 \\
\dot{x}_5 &= 1 - x_5
\end{aligned} \tag{61a}$$

$$v = (x_1 + x_2^2 + x_3 + x_4^2 + x_5)\, i \triangleq R(x_1, x_2, x_3, x_4, x_5)\, i. \tag{61b}$$

The block diagram for this system is shown in Fig. 13. The steady state component of $R(x(t))$ of the zero-state solution $x(t)$ due to the input current $i(t) = A_0 + A\cos\omega t$ has been found analytically and is given by

$$\begin{aligned}
\rho_s(t) &\triangleq R(x(t)) \\
&= a_0(A_0, A, \omega) + \sum_{n=1}^{4} \{a_n(A_0, A, \omega)\cos n\omega t \\
&\quad + b_n(A_0, A, \omega)\sin n\omega t\}
\end{aligned} \tag{62}$$

[20] This choice is to ensure that for any input frequency the canonical model is capable of detecting the components of the input signal correctly in steady state. Otherwise, the solutions x_3 and x_4 in (42a) may never reach the steady state and hence fail to detect the peak values of $u - x_1$ and $-x_2$.

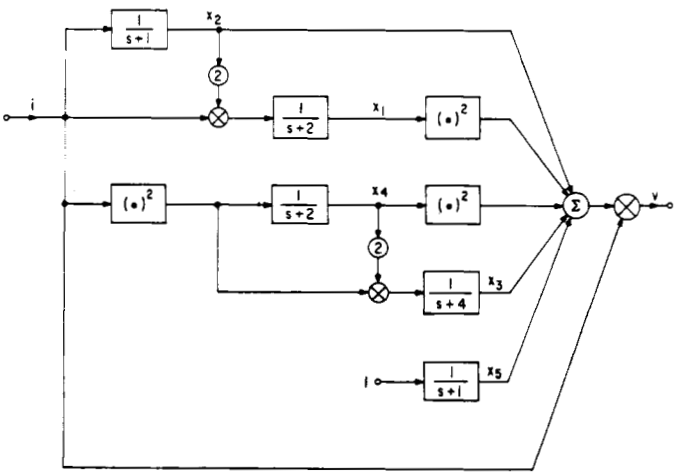

Fig. 13. The block diagram for the hypothetical example in Section III.

where

$$a_0(A_0, A, \omega) = 1 + 2A_0^2 + \frac{1}{2}A_0^4 + \frac{1}{2}A_0^2A^2 + \frac{1}{8}A^4 + \frac{A^2}{\omega^2+1} + 4\left(\frac{A_0A\omega}{\omega^2+4}\right)^2 + 16\left(\frac{A_0A}{\omega^2+4}\right)^2 + \frac{A^4}{16(\omega^2+1)} \tag{63}$$

$$a_1(A_0, A, \omega) = 4\,\frac{A_0A}{\omega^2+1} + 4(A_0^2 + A^2)\,\frac{A_0A}{\omega^2+4} + \frac{A_0A^3(\omega^2+2)}{(\omega^2+1)(\omega^2+4)} \tag{64}$$

$$a_2(A_0, A, \omega) = \frac{A^2(1-\omega^2)}{(\omega^2+1)^2} + \left(\frac{A_0^2}{2} + \frac{A^2}{4}\right)\frac{A^2}{\omega^2+1} + \frac{2A_0^2A^2(4-\omega^2)}{(\omega^2+4)^2} \tag{65}$$

$$a_3(A_0, A, \omega) = \frac{A_0A^3(2-\omega^2)}{(\omega^2+1)(\omega^2+4)} \tag{66}$$

$$a_4(A_0, A, \omega) = \frac{A^4(1-\omega^2)}{16(\omega^2+1)^2} \tag{67}$$

$$b_1(A_0, A, \omega) = \frac{4A_0A\omega}{\omega^2+1} + (4A_0^2 + 2A^2)\,\frac{A_0A\omega}{\omega^2+4} + \frac{A_0A^3\omega}{(\omega^2+1)(\omega^2+4)} \tag{68}$$

$$b_2(A_0, A, \omega) = \frac{4A^2\omega}{\omega^2+1} + \left(A_0^2 + \frac{A^2}{2}\right)\frac{\omega}{\omega^2+1} + \frac{16A_0^2A^2\omega}{(\omega^2+4)^2} \tag{69}$$

$$b_3(A_0, A, \omega) = \frac{3A_0A^3\omega}{(\omega^2+1)(\omega^2+4)} \tag{70}$$

$$b_4(A_0, A, \omega) = \frac{A^4\omega}{4(\omega^2+1)^2}. \tag{71}$$

The model parameters and model functions were identified from the above data and from the system response to the in-

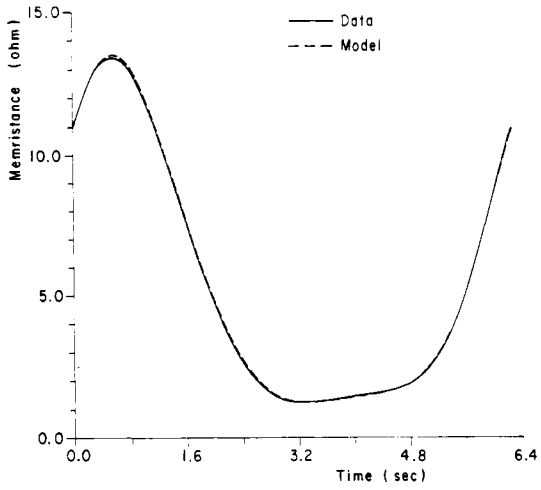

Fig. 14. The steady state model response versus system response.

put testing signals

$$\mathcal{U}_D = \{i(t) = A_{0i} + A_j \cos \omega_k t \mid A_{0i}, A_j \in \{1, 2, 3, 4, 5\}, \omega_k \in \{1, 2, 3, 10^4\}\}.$$

The high "testing frequency" $\omega = 10\,000$ is used to segregate the frequency independent component of the Fourier coefficient $a_0(A_0, A, \omega)$ in (63) (see footnote 16). The *model parameters* determined by the algorithm subject to $\eta_{\max} = 0.5$ is found to be

$$(M, \alpha) = (3, 1/15\pi). \tag{72}$$

There are a total of 28 *nonlinear model functions*. Observe that if the Fourier coefficients contain no frequency independent components then only 27 (i.e., $(2N+1)M$, where $N = 4$, $M = 3$) nonlinear model functions need be identified. The final nonlinear function $g(\cdot)$ for this model is given as follows:

$$\begin{aligned} & g(x_1, x_2, x_3, x_4, i) \\ & \triangleq \nu(x_1, x_3) + \sum_{l=1}^{M=3} \zeta_{0l}(x_1, x_3)\, a_{1l}\left(\left(1 + \frac{\pi}{2}\right)\frac{x_3}{x_4}\right) \\ & \quad + \sum_{n=1}^{N} \left\{\left[\sum_{l=1}^{M=3} \gamma_{nl}(x_1, x_3)\, a_{nl}\left(\left(1 + \frac{\pi}{2}\right)\frac{x_3}{x_4}\right)\right] T_n\left(\frac{i - x_1}{x_3}\right)\right. \\ & \quad + \left[\sum_{l=1}^{M=3} \delta_{nl}(x_1, x_3)\, b_{nl}\left(\left(1 + \frac{\pi}{2}\right)\frac{x_3}{x_4}\right)\right] \\ & \quad \left. \cdot \left(\left(1 + \frac{\pi}{2}\right)\frac{x_2}{x_4} + \frac{\pi}{2}\right) U_{n-1}\left(\frac{i - x_1}{x_3}\right)\right\} \end{aligned} \tag{73}$$

where the nonlinear model functions $\gamma(\cdot)$, $\zeta_{0l}(\cdot)$, $\gamma_{nl}(\cdot)$, and $\delta_{nl}(\cdot)$ are identified using the preceding algorithm. Standard computer optimization techniques are then used to fit the data points defining each model function into a two-dimensional polynomial in x_1 and x_3. The complete descriptions for these functions are listed in Appendix B.

To verify that the model can indeed mimic the original system for any input signal that belongs to the set $\mathcal{U}_D$, we compute the *predicted* steady state response $\hat{\rho}_s(t)$ using the model as well as the *exact* steady state response $\rho_s(t)$ of the given system due to an input $i(t) = A_0 + A \cos \omega t$, where $(A_0, A, \omega) = (1, 1, 1)$. The resulting waveforms of $\hat{\rho}_s(t)$ (dotted curve) and $\rho_s(t)$ (solid curve) are shown in Fig. 14. Note the remarkable resemblance between the two waveforms. To further illustrate the properties of the model, we choose an arbitrary (not a member of $\mathcal{U}_D$) sinusoidal input $i(t) = A \cos \omega t$ with $A = 1$. The frequency dependence of the Lissajous figures of both the model (dotted curve) and the original system (solid curve) is shown in Fig. 15. Observe that as the excitation frequency increases the Lissajous figures of the model and those of the original system shrink and tend to a straight line passing through the origin. The dc characteristic curves of the model (dotted curve) and that of the original system (solid curve) are depicted in Fig. 16. The model was also tested using a *triangular* input signal of period 2π defined as follows:

$$i(t) = \begin{cases} -\dfrac{2}{\pi}\left(t - \dfrac{\pi}{2}\right), & \text{for } t \in [0, \pi] \\ \dfrac{2}{\pi}\left(t - \dfrac{3}{2}\pi\right), & \text{for } t \in [\pi, 2\pi]. \end{cases} \tag{74}$$

The output voltage waveform of the model (dotted curve) and

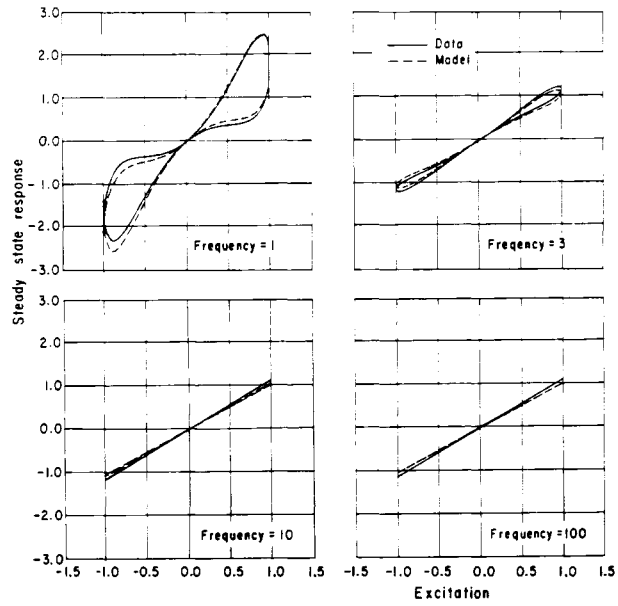

Fig. 15. Frequency dependence of Lissajous figures for the model (dotted curve) and the system (solid curve).

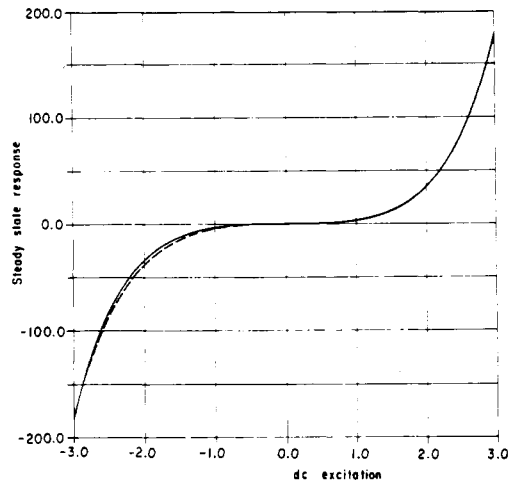

Fig. 16. The dc characteristics of the model (dotted curve) and the system (solid curve).

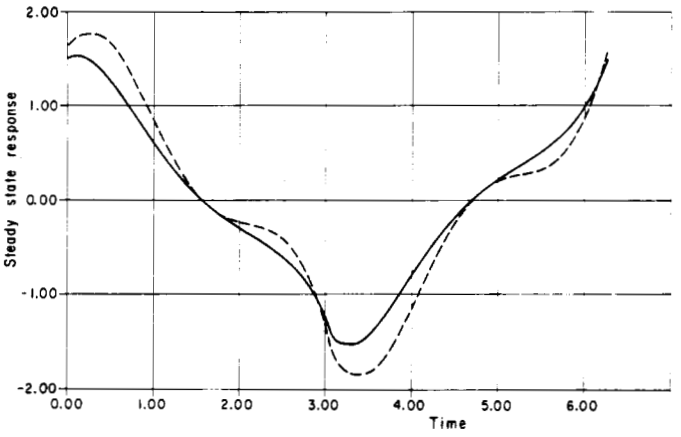

Fig. 17. The response due to a triangular input for the model (dotted curve) and the system (solid curve).

that of the original system (solid curve) are shown in Fig. 17. Observe that there is a close similarity between the two waveforms in spite of the fact that the input signal is *not* a member of the class of input signals $\mathcal{U}$ defined in (30).

IV. Conclusions

A broad generalization of memristors to an interesting class of nonlinear devices and systems called memristive systems has been presented. The most salient feature of memristive systems is its *zero-crossing* property. Observe that in spite of the memory effect which normally introduces phase shifts in conventional systems, the output of a memristive system is zero whenever the input is zero and hence the input–output Lissajous figure always passes through the origin. Roughly speaking, therefore, we could say that a memristive system is a "zero phase shift" dynamic system. Various generic properties of memristive systems have been derived and shown to coincide with those possessed by many physical devices and systems. Among the various properties of memristive systems, the frequency response of the Lissajous figure is especially interesting. As the excitation frequency increases toward infinity, the Lissajous figure shrinks and tends to a straight line passing through the origin—except for some pathological cases where the bibs stability property is not satisfied. The physical interpretation of this phenomenon is that the system possesses certain inertia and cannot respond as rapidly as the fast variation in the excitation waveform and therefore must settle to some equilibrium state. This implies that the hysteretic effect of the memristive system decreases as the frequency increases and hence it eventually degenerates into a purely *resistive* system. Under small-signal operations, the memristive one-port can be either *inductive* or *capacitive* depending on the biasing point.

We believe that many devices and systems which have so far been identified as *dissipative* should actually be modeled as *memristive systems*. Only by using such a model can the *dynamic behavior* be properly simulated. Finally, we remark that *the model presented can be made exact under dc, small-signal (for all operating points) or sinusoidal (with dc component) excitations*. Even though our canonical model contains a time-varying component in the state equations; namely $\dot{x}_1 = a(t)x_1 + b(t)u$, we observe that both $a(t)$ and $b(t)$ tend to zero in steady state. Hence, under steady-state operation, our canonical model degenerates into a *time-invariant dynamical system*. Furthermore, if the class of input testing signals is confined to only purely sinusoidal waveforms, then our canonical model can be drastically simplified to a dynamical system characterized by a *third-order time-invariant* state equation and a much simpler output equation.

Appendix A

Lemma A.1

The scalar functions $\zeta_{0l}(\cdot)$, $\gamma_{kl}(\cdot)$, and $\delta_{kl}(\cdot)$ defined via (44)–(46) are continuous functions of $(A_0, A) \in \mathcal{R} \times \mathcal{R}_+$.

Proof: From (44),

$$\gamma_{kl}(A_0, A) - \gamma_{kl}(\hat{A}_0, \hat{A}) = \int_{1/k}^{\infty} \left(a_k(A_0, A, \omega) - a_k(\hat{A}_0, \hat{A}, \omega)\right) a_{kl}(\omega)\, d\omega. \quad (A.1)$$

From (A.1) and the Schwarz inequality, we obtain

$$|\gamma_{kl}(A_0, A) - \gamma_{kl}(\hat{A}_0, \hat{A})| \leq \left[\int_{1/k}^{\infty} |a_k(A_0, A, \omega) - a_k(\hat{A}_0, \hat{A}, \omega)|^2\, d\omega\right]^{1/2} \left[\int_{1/k}^{\infty} |a_{kl}(\omega)|^2\, d\omega\right]^{1/2}. \quad (A.2)$$

The normality of $a_{kl}(\cdot)$ implies that

$$|\gamma_{kl}(A_0, A) - \gamma_{kl}(\hat{A}_0, \hat{A})| \leq \left[\int_{1/k}^{\infty} |a_k(A_0, A, \omega) - a_k(\hat{A}_0, \hat{A}, \omega)|^2\, d\omega\right]^{1/2}. \quad (A.3)$$

Since $a_k(\cdot, \cdot, \omega)$ are mean-square continuous (see (36)), by assumption, $\gamma_{kl}(\cdot)$ is continuous in $(A_0, A) \in \mathcal{R} \times \mathcal{R}_+$. Similar arguments reveal that $\zeta_{0l}(\cdot)$ and $\delta_{kl}(\cdot)$ are continuous in $(A_0, A) \in \mathcal{R} \times \mathcal{R}_+$. ■

Lemma A.2

The *steady-state solution* of

$$\dot{x}_1 = -a(t)\, x_1 + b(t)\, u \quad (A.4)$$

where $u(t) = A_0 + A \cos \omega t$, $x_1(0) = 0$ tends to a constant A_0.

Proof: In (A.4), $a(t)$ and $b(t)$ are given by (42c); namely,

$$a(t) = \frac{1 - e^{-Kt}}{t + (1/K)\, e^{-Kt}} \text{ and } b(t) = \frac{1}{t + (1/K)\, e^{-Kt}}, \quad K \gg 1.$$

Hence, the function $t \mapsto -a(t)\, x_1 + b(t)\, u(t)$ is continuous and the function $x_1 \mapsto -a(t)\, x_1 + b(t)\, u$ is Lipschitz continuous with continuous Lipschitz function on $\mathcal{R}_+$. By the fundamental theorem of differential equations [5], [17], there exists a unique solution $x_1(t)$ on $\mathcal{R}_+$ (for $x_1(0) = 0$)

$$x_1(t) = \frac{1}{t + (1/K)\, e^{-Kt}} \int_0^t u(\tau)\, d\tau. \quad (A.5)$$

It follows from (A.5) that $x_1(t)$ corresponding to $u(t) = A_0 + A \cos \omega t$ tends to A_0, i.e., $x_1(t) \to A_0$ as $t \to \infty$. ■

Lemma A.3

Consider the first-order differential equation

$$\dot{x}_3 = p(u - x_1 - x_3), \quad x_3(0) = 0 \quad (A.6)$$

where the nonlinear function $p(\cdot)$ is defined by (49), x_1 is the solution of (A.4) and $u(t) = A_0 + A\cos\omega t$. Then for each $\epsilon > 0$, there exists a $\hat{\delta} \in (0, 1)$ such that for any $\alpha \in (0, \hat{\delta})$, the solution $x_3(t)$ tends to a constant A; namely

$$\lim_{t\to\infty} |x_3(t) - A| < \epsilon. \tag{A.7}$$

Proof: From Lemma A.2 the steady-state component of $x_1(t)$ is A_0. Hence for $t \geqslant t_0$, where t_0 is a sufficiently large number, (A.6) is equivalent to

$$\dot{x}_3 = p(\tilde{u} - x_3) \tag{A.8}$$

where $\tilde{u}(t) = A\cos\omega t$. The inequality (A.7) follows from (A.8). For a proof of this assertion see [15]. ∎

Remark: The differential equation (A.8) describes a *peak detector* and in steady state[21] the solution $x_3(t)$ for an arbitrary initial condition is arbitrarily close to the peak value of *any* periodic waveform $\tilde{u}(\cdot)$.

Theorem A.1

Given any $\epsilon > 0$, there exists a $\delta \in (0, 1)$ such that for any $\alpha \in (0, \delta)$, and for any input signal $u(t) = A_0 + A\cos\omega t$ the *steady-state solutions* to (42a) satisfy the following inequalities:

$$|x_1 - A_0| < \epsilon \tag{A.9}$$

$$|x_3 - A| < \epsilon \tag{A.10}$$

$$\left|\left(1 + \frac{\pi}{2}\right)\frac{x_3}{x_4} - \omega\right| < \epsilon \tag{A.11}$$

$$\left|\left(1 + \frac{\pi}{2}\right)\frac{x_2}{x_4} + \frac{\pi}{2} - \sin\omega t\right| < \epsilon \tag{A.12}$$

$$\left|\frac{u - x_1}{x_3} - \cos\omega t\right| < \epsilon. \tag{A.13}$$

Proof: The inequalities (A.9) and (A.10) follow from Lemma A.2 and Lemma A.3, respectively. Consider the differential equation for x_2 in (42a); namely,

$$\dot{x}_2 = -x_1 + u,\ x_2(0) = 0. \tag{A.14}$$

It follows from (A.5) and $u(t) = A_0 + A\cos\omega t$ that

$$\begin{aligned} x_2(t) &= \int_0^t \left(u(\tau) - \frac{1}{\tau + (1/K)\,e^{-K\tau}} \int_0^\tau u(s)\,ds\right) d\tau \\ &= \int_0^t \left(\frac{A_0}{K}\,\frac{e^{-K\tau}}{t + (1/K)\,e^{-K\tau}} + A\cos\omega\tau \right. \\ &\quad \left. - \frac{A}{\omega}\,\frac{\sin\omega\tau}{\tau + (1/K)\,e^{-K\tau}}\right) d\tau \\ &= \frac{A}{\omega}\sin\omega t + \frac{A_0}{K}\int_0^t \frac{1}{1 + \tau e^{\tau}} \\ &\quad - \frac{A}{\omega}\int_0^t \frac{\sin\omega\tau}{\tau + (1/K)\,e^{-K\tau}}\,d\tau. \end{aligned} \tag{A.15}$$

Applying (A.15) and the triangle inequality, we obtain

$$\begin{aligned} &\left|x_2(t) - \frac{A}{\omega}\left(\sin\omega t - \int_0^t \frac{\sin\omega\tau}{\tau}\,d\tau\right)\right| = \left|\frac{A_0}{K}\int_0^t \frac{1}{1 + \tau e^{\tau}}\,d\tau \right. \\ &\left. - \frac{A}{\omega}\int_0^t \left(\frac{\sin\omega\tau}{\tau + (1/K)\,e^{-K\tau}} - \frac{\sin\omega\tau}{\tau}\right) d\tau\right| \\ &\leqslant \frac{A_0}{K}\int_0^t \frac{1}{1 + \tau e^{\tau}}\,d\tau + \frac{A}{\omega}\int_0^t \left|\frac{\sin\omega\tau}{\tau + (1/K)\,e^{-K\tau}} - \frac{\sin\omega\tau}{\tau}\right| d\tau \\ &< \frac{A_0 + \omega}{K}\,\frac{1 + e}{e} \end{aligned} \tag{A.16}$$

(where $e = 2.71828\cdots$) for all $t \in \mathcal{R}_+$. Since the integral

$$\int_0^t \frac{\sin\omega\tau}{\tau}\,d\tau \to \frac{\pi}{2} \text{ as } t \to \infty$$

for sufficiently large K and for sufficiently large t, the solution $x_2(t)$ in steady state is such that

$$x_2(t) \cong \frac{A}{\omega}\left(\sin\omega t - \frac{\pi}{2}\right). \tag{A.17}$$

Hence as K and t increase toward infinity, $x_2(t)$ becomes *almost periodic*.[22] In (42a) the solution of

$$x_4 = p(-x_2 - x_4),\ x_4(0) = 0 \tag{A.18}$$

is almost periodic in steady state when $x_2(t)$ is almost periodic because $x_4(t)$ is bounded on $\mathcal{R}_+$ and the function $t \mapsto p(-x_2(t) - x_4)$ is almost periodic [17]. By a similar argument used in the proof of Lemma A.3, we can assert that given any $\epsilon > 0$ there exists a $\delta_4 \in (0, 1)$ such that for any $\alpha \in (0, \delta_4)$, the steady-state component of $x_4(t)$ is arbitrarily close to the peak value of $-x_2(t)$, i.e.,

$$\lim_{t\to\infty} \left|x_4(t) - \left(1 + \frac{\pi}{2}\right)\frac{A}{\omega}\right| < \epsilon. \tag{A.19}$$

Let $\delta_3 \in (0, 1)$ denote the associated constant so that for any $\alpha \in (0, \delta_3)$ the inequality (A.10) is satisfied. If we choose $\delta = \min\{\delta_3, \delta_4\}$, then the inequality (A.11) follows from inequalities (A.10) and (A.19). Similarly, the inequality (A.12) follows from (A.17) and inequality (A.19). The last inequality (A.13) follows from the inequalities (A.9) and (A.10). ∎

Appendix B

The nonlinear model functions $\nu(x_1, x_3)$, $\zeta_{0l}(x_1, x_3)$, $\gamma_{nl}(x_1, x_3)$, and $\delta_{nl}(x_1, x_3)$ are described in terms of two-dimensional polynomials of the form

$$P(x_1, x_3) = \sum_{i=1}^{N_i=5}\ \sum_{j=1}^{N_j=5} a_{ij}\, x_1^{i-1}\, x_3^{j-1}. \tag{B.1}$$

Observe that for each nonlinear model function there are 25 polynomial coefficients. The list of these coefficients is as shown in Table I, where a_{ij} is located at the ith row and the jth column associated with each function. These coefficients were determined using the Fletcher-Powell minimization algorithm [18].

[21] By steady state we mean that the transient component is negligible.

[22] A function $f(t)$ is said to be *almost periodic* if for any $\eta > 0$, there is an $l = l(f, \eta) > 0$ such that in any interval of length l there is a τ such that $|f(t + \tau) - f(t)| < \eta$ for all $t \in \mathcal{R}$.

TABLE I

	(a_{ij})						(a_{ij})				
$\nu(x_1,x_3)$	.749	.024	.199	-.087	.135	$\gamma_{42}(x_1,x_3)$	-.022	.045	-.029	.007	34.719
	.662	-.410	-.150	.108	-.013		.038	-.078	.051	-.013	.001
	1.510	.420	.485	-.040	.006		-.021	.045	-.029	.007	-.001
	.134	-.132	.023	.005	-.001		.005	-.010	.007	-.002	.000
	.488	.013	-.003	-.000	.000		-.000	.001	-.001	.000	-.000
$\zeta_{01}(x_1,x_3)$	.407	-.073	.708	.127	.048	$\gamma_{43}(x_1,x_3)$	.219	-.403	.298	-.087	-313.336
	-.388	-.537	.923	-.330	.034		-.351	.657	-.504	.151	-.015
	.057	.643	2.764	.243	-.024		.196	-.373	.293	-.089	.009
	.018	-.212	.212	-.066	.006		-.045	.087	-.069	.021	-.002
	-.003	.021	-.020	.006	-.001		.004	-.007	.006	-.002	.000
$\zeta_{02}(x_1,x_3)$	.295	-.545	-.524	-.078	-.047	$\delta_{11}(x_1,x_3)$	-.379	.766	-.499	.127	-.011
	-.545	1.008	-.602	.143	-.012		.848	2.291	1.065	1.524	.023
	.326	-.602	-6.779	-.086	.007		-.583	1.131	-.712	.177	-.015
	-.078	.143	-.086	.020	-.002		.154	3.213	.184	-.045	.004
	.006	-.012	.007	-.002	.000		-.014	.026	-.016	.004	-.000
$\zeta_{03}(x_1,x_3)$	.162	.059	.219	.047	.018	$\delta_{12}(x_1,x_3)$	-.064	-.193	.269	-.092	.009
	.016	-.689	.606	-.170	.015		-.618	-1.681	-1.310	-2.893	-.033
	-.092	.564	3.977	.124	-.011		.724	-1.682	1.174	-.311	.028
	.031	-.152	.119	-.032	.003		-.237	-6.617	-.351	.091	-.008
	-.003	.013	-.010	.003	-.000		.024	-.050	.033	-.009	.001
$\gamma_{11}(x_1,x_3)$	.056	.335	-.416	.139	-.014	$\delta_{13}(x_1,x_3)$	.121	-.026	-.081	.037	-.004
	.625	1.992	1.575	3.973	.042		.249	.615	.671	1.774	.018
	-.726	1.827	-1.329	.361	-.032		-.375	.911	-.650	.174	-.016
	.238	6.461	.388	-.103	.009		.131	4.137	.200	-.052	.005
	-.024	.053	-.036	.010	-.001		-.013	.029	-.019	.005	-.000
$\gamma_{12}(x_1,x_3)$	-.633	.273	.271	-.144	.017	$\delta_{21}(x_1,x_3)$	-.076	.139	.094	.019	.246
	-.361	-1.074	-2.190	-7.943	-.064		.139	-.255	.151	-.036	.003
	.947	-2.741	2.115	-.592	.054		-.083	.151	1.776	.021	-.002
	-.359	-13.377	-.651	.176	-.016		.020	-.036	.021	-.005	.000
	.038	-.090	.063	-.017	.001		-.002	.003	-.002	.000	-.000
$\gamma_{13}(x_1,x_3)$	-.317	.619	-.394	.097	-.008	$\delta_{22}(x_1,x_3)$	-1.155	2.134	19.845	.304	-.875
	.616	.243	.760	5.102	.016		2.134	-3.944	2.355	-.561	.046
	-.421	.811	-.511	.125	-.010		-1.275	2.356	10.435	.335	-.028
	.115	8.642	.137	-.033	.003		.304	-.561	.335	-.080	.007
	-.011	.020	-.013	.003	-.000		-.025	.046	-.028	.007	-.001
$\gamma_{21}(x_1,x_3)$	.160	-.464	-3.412	-.107	1.000	$\delta_{23}(x_1,x_3)$	3.796	-7.071	-51.057	-1.011	1.523
	-.211	.701	-.595	.176	-.017		-7.021	13.078	-7.839	1.870	-.154
	.103	-.376	-1.964	-.099	.009		4.185	-7.797	-48.070	-1.115	.092
	-.022	.085	-.075	.023	-.002		-.994	1.853	-1.111	.265	-.022
	.002	-.007	.006	-.002	.000		.082	-.152	.091	-.022	.002
$\gamma_{22}(x_1,x_3)$	-4.058	7.499	30.242	1.067	-3.488	$\delta_{31}(x_1,x_3)$	.015	.009	-.023	.009	-.001
	7.499	-13.859	8.276	-1.971	.162		-.028	-.016	.043	.323	.002
	-4.478	8.276	72.450	1.177	-.097		.017	.009	-.025	.010	-.001
	1.067	-1.971	1.177	-.280	.023		-.004	-.002	.006	-.002	.000
	-.088	.162	-.097	.023	-.002		.000	.000	-.000	.000	-.000
$\gamma_{23}(x_1,x_3)$	11.616	-21.466	-65.517	-3.053	6.011	$\delta_{32}(x_1,x_3)$	-.375	.694	-.414	.099	-.008
	-21.467	39.671	-23.690	5.642	-.464		.694	-1.282	.765	25.052	.015
	12.820	-23.691	-227.364	-3.369	.277		-.414	.765	-.457	.109	-.009
	-3.053	5.642	-3.369	.802	-.066		.099	-.182	.109	-.026	.002
	.251	-.464	.277	-.066	.005		-.008	.015	-.009	.002	-.000
$\gamma_{31}(x_1,x_3)$	-.306	-.187	.474	-.179	.019	$\delta_{33}(x_1,x_3)$	2.702	-4.993	2.982	-.710	.058
	.574	.331	-.867	-6.546	-.035		-4.993	9.228	-5.511	-180.377	-.108
	-.346	-.191	.514	-.196	.021		2.982	-5.511	3.291	-.784	.064
	.083	.044	-.122	.046	-.005		-.710	1.313	-.784	.187	-.015
	-.007	-.004	.010	-.004	.000		.058	-.108	.064	-.015	.001
$\gamma_{32}(x_1,x_3)$	-3.257	6.021	-3.595	.856	-.070	$\delta_{41}(x_1,x_3)$	.000	.000	-.000	.000	.022
	6.022	-11.127	6.641	218.677	.130		-.000	-.000	.000	-.000	.000
	-3.598	6.645	-3.965	.943	-.078		.000	-.000	-.000	.000	-.000
	.857	-1.583	.944	-.225	.018		-.000	.000	.000	-.000	.000
	-.070	.130	-.078	.018	-.002		.000	-.000	.000	.000	-.000
$\gamma_{33}(x_1,x_3)$	19.779	-34.663	24.536	-6.979	.662	$\delta_{42}(x_1,x_3)$	.011	.049	-.063	.021	10.558
	-37.749	66.006	-46.361	-1339.469	-1.238		-.056	-.023	.075	-.029	.003
	22.109	-38.421	26.992	-7.640	.723		.051	-.019	-.025	.013	-.001
	-5.087	8.778	-6.185	1.757	-.167		-.016	.011	.002	-.002	.000
	.403	-.691	.489	-.139	.013		.001	-.001	.000	.000	-.000
$\gamma_{41}(x_1,x_3)$	.001	-.001	.001	-.000	-.946	$\delta_{43}(x_1,x_3)$	-.106	-.508	.641	-.217	-110.570
	-.001	.002	-.002	.000	-.000		.572	.243	-.769	.301	-.032
	.000	-.001	.001	-.000	.000		-.524	.190	.259	-.132	.015
	-.000	.000	-.000	.000	-.000		.158	-.107	-.025	.023	-.003
	.000	-.000	.000	-.000	.000		-.015	.013	-.000	-.001	.000

REFERENCES

[1] L. O. Chua, "Memristors–the missing circuit element," *IEEE Trans. Circuit Theory*, vol. CT-18, pp. 507–519, Sept. 1971.

[2] G. F. Oster and D. M. Auslander, "The memristor: A new bond graph element," *Trans. ASME on Dynamical Syst. Meas. Contr.*, vol. 94, no. 3, pp. 249–252, 1972.

[3] G. F. Oster, "A note on memristor," *IEEE Trans. Circuits Syst.*, vol. CAS-21, p. 152, Jan. 1974.

[4] L. O. Chua and C. W. Tseng, "A memristive circuit model for P-N junction diodes," *Int. J. Circuit Theory and Appl.*, vol. 2, pp. 367–389, Dec. 1974.

[5] C. A. Desoer, *Notes for a Second Course on Linear Systems*. New York: Van Nostrand Reinhold, 1970.

[6] L. O. Chua, *Introduction to Nonlinear Circuit Theory*. New York: McGraw-Hill, 1969.

[7] M. Sapoff and R. M. Oppenheim, "Theory and application of self-heated thermistors," *Proc. IEEE*, vol. 51, pp. 1292–1305, Oct. 1963.

[8] A. L. Hodgkin and A. F. Huxley, "A quantitative description of membrane current and its application to conduction in nerve," *J. Physiol.*, vol. 117, pp. 500–544, 1952.

[9] V. J. Francis, *Fundamentals of Discharge Tube Circuits*. London, England: Methuen, 1948.

[10] J. C. Willems, "Dissipative dynamical systems Part I: General theory," *Arch. Rational Mech. Anal.*, vol. 45, pp. 321–351, Apr.–May 1972.

[11] W. Hahn, *Stability of Motion*. New York: Springer Verlag, 1967.

[12] A. Mauro, "Anomalous impedance, a phenomenological property of time-variant resistance," *Biophys. J.*, vol. 1, pp. 353–372, 1961.

[13] L. Weinberg, *Network Analysis and Synthesis*. New York: McGraw-Hill, 1962.

[14] A. L. Reenstra, "A low-frequency oscillator using PTC and NTC thermistors," *IEEE Trans. Electron Devices*, vol. ED-16, pp. 544–554, June 1969.

[15] L. O. Chua and R. J. Schilling, "An algorithm for modeling the sinusoidal input/steady state response behavior of nonlinear systems over a set of frequencies and amplitudes," *J. Franklin Inst.*, vol. 298, no. 2, pp. 101–124, Aug. 1974.

[16] L. Fox and I. B. Parker, *Chebyshev Polynomials in Numerical Analysis*. London, England: Oxford Univ. Press, 1968.

[17] J. K. Hale, *Ordinary Differential Equations*. New York: Wiley-Interscience, 1969.

[18] R. Fletcher and M. J. D. Powell, "A rapidly convergent descent method of minimization," *British Comput. J.*, vol. 6, pp. 163–168, 1963.